

Improving imaging resolution of shaking targets by Fourier-transform ghost diffraction

Cong Zhang, Wenlin Gong,* and Shensheng Han

Key Laboratory for Quantum Optics and Center for Cold Atom Physics of CAS,
Shanghai Institute of Optics and Fine Mechanics,
Chinese Academy of Sciences, Shanghai 201800, China

(Dated: November 6, 2018)

For conventional imaging, shaking of the imaging system or the target leads to the degradation of imaging resolution. In this work, the influence of the target's shaking to Fourier-transform ghost diffraction (FGD) is investigated. The analytical results, which are backed up by numerical simulation and experiments, demonstrate that the quiver of target has no effect on the resolution of FGD, thus the target's imaging with high spatial resolution can be always achieved by phase-retrieval method from the FGD patterns. This approach can be applied in high-precision imaging systems, to overcome the influence of the system's shaking to imaging resolution.

PACS numbers: 42.25.Kb, 42.50.Ar, 42.30.Va

Relative motion between the imaging system and the object is one of the common reasons for imaging degradation. For instance, camera's shaking or object's high-speed moving would cause the blur and degradation of imaging resolution. For conventional imaging, a usual method to decrease motion blur is to reduce the exposure time, while this will reduce the signal-to-noise ratio (SNR) of the images.

Other approaches for motion deblurring include mechanical compensation, optical compensation and electrical compensation [1, 2]. However, the imaging resolution is limited by the compensation accuracy. Also, the designing and manufacturing of compensation devices are complex and the development of compensation techniques is still one of the most challenging tasks.

Motion deblurring can also be completed by digital image processing method [3]. The blur kernel, namely point spread function, is the key factor in the process of image restoration. If the blur kernel is known before image restoration, inverse filtering and Wiener filtering are widely used for image restoration [4–6]. If the blur kernel cannot be known or measured in some practical applications, image restoration is usually realized by blind deconvolution technique [7–9]. However, image restoration needs large computation and suffers from serious restoration errors, moreover it is sensitive to noise disturbance.

Ghost imaging (GI), as a nonlocal imaging method, has been widely investigated during last fifteen years [10–17]. An interesting and obvious feature of ghost imaging is that Fourier-transform imaging of the object can be obtained by measuring the intensity correlation function between two light fields, even when the source is a thermal light source and the object is located in Fresnel region relative to the source [17–22]. Recently, super-resolution far-field ghost imaging and ghost imaging lidar are also obtained by exploiting the sparsity constraints of images [23–25]. However, all the previous work on ghost imag-

ing is focused on the static targets. Obviously, imaging an unstable and moving target is meaningful in practice. Based on the lensless Fourier-transform ghost diffraction (FGD) scheme [20] and phase-retrieval techniques [21], the effect of the target's shaking on FGD is investigated both theoretically and experimentally, and the target's imaging is retrieved from the experimental FGD patterns. We show that the scheme is helpful in overcoming the shaking blur due to the novel characteristic of ghost imaging technique.

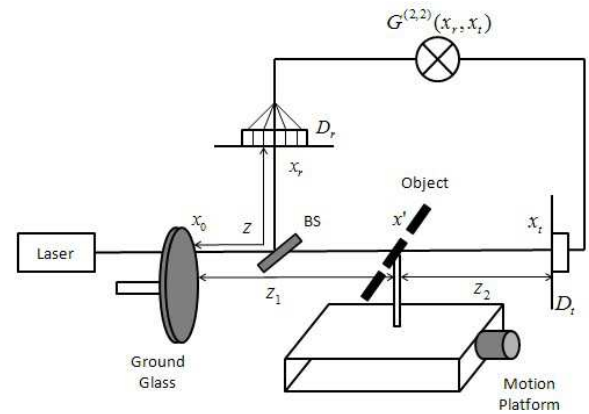


FIG. 1: Schematic of lensless FGD for shaking targets with pseudo-thermal light. The object is operated by a motion platform so that it can shake on the object plane, perpendicular to the optical axis.

Fig. 1 presents the experimental schematic of lensless FGD for shaking targets with pseudo-thermal light. The pseudo-thermal source, which is obtained by modulating a laser beam (the wavelength $\lambda=532$ nm and the light spot's transverse size $D=4$ mm) with a rotating ground glass, is divided by a beam splitter (BS) into a test and a reference paths. In the reference path, the light propagates directly to a charge-coupled device (CCD) camera D_r . In the test path, the light goes through an object and then to a single pointlike detector D_t . The object is

*Electronic address: gongwl@siom.ac.cn

placed on a motion platform and the platform is driven by a stepping motor so that it can move straight in one dimension. In addition, the stepping accuracy of the platform is $5 \mu m$ and the stepping motor is connected to a

computer, which can control the motion of the object.

Based on GI theory [15, 17], the correlation function between the two detectors is

$$\begin{aligned} \Delta G^{(2,2)}(x_r, x_t) &= \langle E_r(x_r) E_r^*(x_r) E_t^*(x_t) E_t(x_t) \rangle - \langle E_r(x_r) E_r^*(x_r) \rangle \langle E_t(x_t) E_t^*(x_t) \rangle \\ &= \int dx_{01} dx_{02} dx_{03} dx_{04} \langle E_0(x_{01}) E_0^*(x_{04}) \rangle \langle E_0^*(x_{02}) E_0(x_{03}) \rangle \\ &\quad \times \langle h_r(x_r, x_{01}) h_t^*(x_t, x_{04}) h_r^*(x_r, x_{02}) h_t(x_t, x_{03}) \rangle, \end{aligned} \quad (1)$$

where $\langle \dots \rangle$ denotes an ensemble average, $E_r(x_r)$ and $E_t(x_t)$ denote the light fields on the reference and test detection planes, respectively. $\langle E_0(x_0) E_0^*(x'_0) \rangle$ is the auto-correlation function of light field on the ground glass plane. $h_t(x_t, x_0)$ is the impulse response function of the test path, whereas $h_r^*(x_r, x_0)$ denotes the phase conjugate of the impulse response function in the reference path.

For the schematic shown in Fig. 1, under the paraxial approximation, the impulse response function of the reference path is

$$h_r(x_r, x_0) \propto \exp\left\{\frac{jk}{2z}(x_r - x_0)^2\right\}, \quad (2)$$

where $k = 2\pi/\lambda$. And the impulse response function for the test path is

$$\begin{aligned} h_t(x_t, x_0) &\propto \int dx' t(x', \tau) \exp\left\{\frac{jk}{2z_1}(x' - x_0)^2\right\} \\ &\quad \times \exp\left\{\frac{jk}{2z_2}(x_t - x')^2\right\}, \end{aligned} \quad (3)$$

where $t(x', \tau)$ is the transmission function of the object at time τ . Assuming that the light field on the ground glass plane is fully spatially incoherent and the intensity distribution is uniform as a constant intensity I_0 , then

$$\begin{aligned} \langle E_0(x_{01}) E_0^*(x_{04}) \rangle &= I_0 \delta(x_{01} - x_{04}), \\ \langle E_0(x_{02}) E_0^*(x_{03}) \rangle &= I_0 \delta(x_{02} - x_{03}), \end{aligned} \quad (4)$$

where $\delta(x)$ is the Dirac delta function.

Substituting Eq. (2)-(4) into Eq. (1) and suppose that $z = z_1 + z_2$, the correlation function is

$$\begin{aligned} \Delta G^{(2,2)}(x_r, x_t) &\propto \int dx'_1 dx'_2 \exp\left\{-\frac{jk}{z_2}(x_r - x_t)x'_1\right\} \\ &\quad \times \langle t(x'_1, \tau) t^*(x'_2, \tau) \rangle \exp\left\{\frac{jk}{z_2}(x_r - x_t)x'_2\right\}, \end{aligned} \quad (5)$$

The object's shaking means that the center position of the object will deviate from the optical axis. If the object's center position deviates ξ from the optical axis at time τ , then the object's transmission function $t(x', \tau)$ will change into $t(x' - \xi)$. In practical applications, although the shaking deviation of the object is unknown

and random at every time, it obeys to a certain statistical distribution. Assume that the shaking deviation ξ obeys to probability distribution $P(\xi)$ (where $\int d\xi P(\xi) = 1$), then

$$\langle t(x'_1, \tau) t^*(x'_2, \tau) \rangle = \int d\xi P(\xi) t(x'_1 - \xi) t^*(x'_2 - \xi), \quad (6)$$

Substituting Eq. (6) into Eq. (5), after some calculations, Eq. (5) can be represented as

$$\begin{aligned} \Delta G^{(2,2)}(x_r, x_t) &\propto \left| \tilde{T}\left(\frac{2\pi}{\lambda z_2}(x_r - x_t)\right) \right|^2 \int d\xi P(\xi) \\ &= \left| \tilde{T}\left(\frac{2\pi}{\lambda z_2}(x_r - x_t)\right) \right|^2, \end{aligned} \quad (7)$$

where $\tilde{T}(q)$ is Fourier transformation of the object $t(x')$. If the detector in the test path is a single pointlike detector which is located at $x_t = 0$, then

$$\Delta G^{(2,2)}(x_r, x_t = 0) \propto \left| \tilde{T}\left(\frac{2\pi}{\lambda z_2} x_r\right) \right|^2. \quad (8)$$

From Eqs. (7) and (8), the object's FGD can be still obtained even if the object is shaking and the result is the same as that achieved in the static condition [17]. Therefore, the object's shaking has no effect on the imaging resolution of FGD.

In order to verify the analytical results, Fig. 2 and Fig. 3, respectively, present the numerical simulated and experimental results of imaging a three-slit in different shaking conditions, using the lensless scheme shown in Fig. 1. In the simulation and experiments, the distances listed in Fig. 1 are as follows: $z = 550$ mm, $z_1 = 200$ mm, $z_2 = 350$ mm. The object is a three-slit with slit width $a = 0.2$ mm, center-to-center separation $d = 1.0$ mm, and slit height $h = 1.0$ mm.

The shaking modes of the object are controlled by the motion platform and two statistical distributions are discussed: uniform and normal. The maximum shaking deviation from the optical axis is $100\mu m$, $500\mu m$, $1000\mu m$, $2000\mu m$, respectively, which is used to perform the influence of the shaking amplitude to the imaging resolution of FGD.

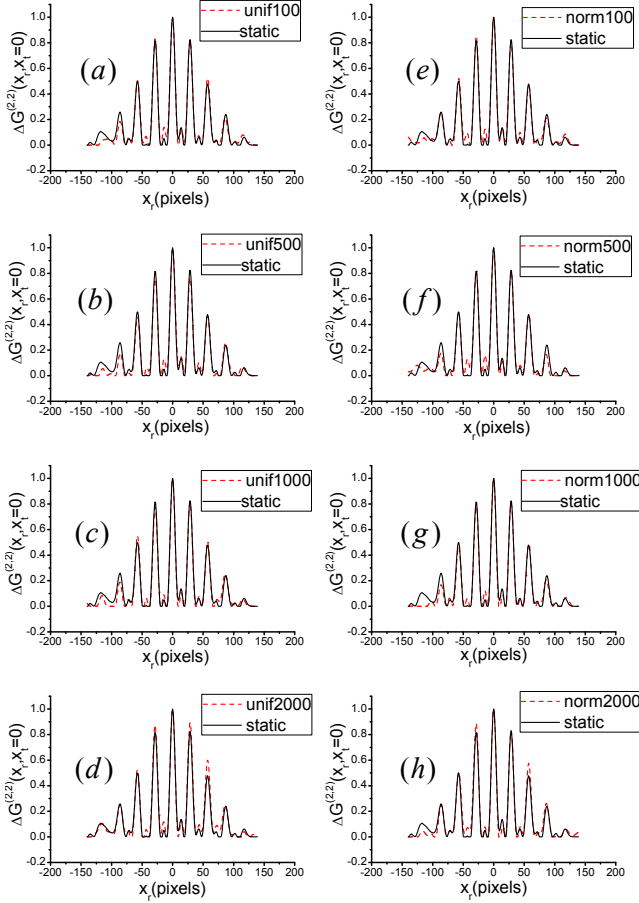


FIG. 2: Numerical simulation results of shaking object FGD with the lensless scheme shown in Fig. 1 (averaged 4000 measurements). X-axis indicates the position on the reference detector D_r . Y-axis indicates FGD reconstructed by measuring the intensity correlation function $\Delta G^{(2,2)}(x_r, x_t = 0)$. (a)-(d): the shaking mode obeys to uniform statistical distribution, and the maximum shaking deviation from the optical axis is $100\mu\text{m}$, $500\mu\text{m}$, $1000\mu\text{m}$, $2000\mu\text{m}$, respectively. (e)-(h): the shaking mode obeys to normal statistical distribution, and the maximum shaking deviation from the optical axis is respectively $100\mu\text{m}$, $500\mu\text{m}$, $1000\mu\text{m}$, $2000\mu\text{m}$. Red dashed curves present FGD reconstructed in different shaking conditions versus black solid curves for the static condition.

For Fig. 2 and Fig. 3, FGD in the static condition is illustrated by black solid curves. If the object's shaking mode obeys to uniform distribution, the results in different shaking amplitudes are shown in Fig. 2(a)-(d) and Fig. 3(a)-(d). While in the case of normal distribution, Fig. 2(e)-(h) and Fig. 3(e)-(h) present the corresponding simulated and experimental results. From the simulated and experimental results shown in Fig. 2 and Fig. 3, both the shaking mode and the shaking amplitudes of the object have no effect on the imaging resolution of FGD and the imaging quality is the same as that in the static case, which is in accordance with the analytical results described by Eqs. (7) and (8).

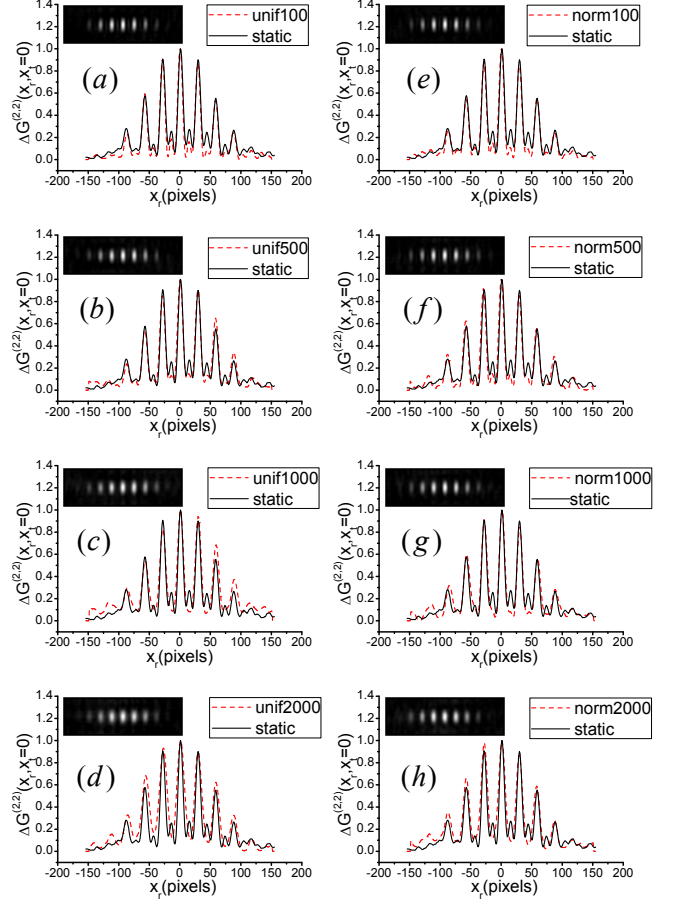


FIG. 3: Experimental results of shaking object FGD, the conditions are the same as Fig. 2. The images in different shaking conditions reconstructed by measuring the intensity correlation function $\Delta G^{(2,2)}(x_r, x_t = 0)$ are listed at the upper left corners and red dashed curves are their cross-sections. In contrast, black solid curves are the cross-section of FGD obtained in the case of static condition.

In addition, based on phase-retrieval iterative algorithm [21], the object's imaging in two shaking modes and different shaking amplitudes, as shown in Fig. 4, can be retrieved from the experimental FGD patterns of Fig. 3. From Fig. 4(d,f) and (i,j), even if the object's shaking amplitude is much larger than center-to-center separation of the object, the spatial resolution of reconstructed object is nearly the same as that retrieved in the static condition when FGD technique and phase-retrieval method are combined, which can overcome the influence of relative motion between the imaging system and the object to imaging resolution in conventional imaging system.

For FGD, a single pointlike detector far from the object in the test path can receive the global information of the object. However, the spectrum center of FGD will move if we change the position x_t of the single pointlike detector, which can be explained by Eq. (7) because the center of the object's FGD is related to the detection po-

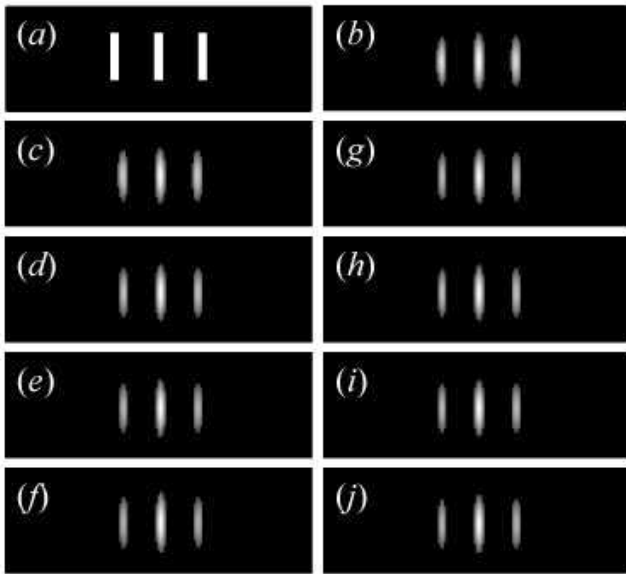


FIG. 4: The object's imaging retrieved from FGD patterns based on the experimental results of Fig. 3. (a) The original object used in numerical simulation and experiments; (b) phase-retrieval image of static object FGD; (c)-(f): corresponding phase-retrieval results of Fig. 4(a)-(d); (g)-(j): corresponding phase-retrieval results of Fig. 4(e)-(h).

sition x_t and the result has also been demonstrated in Ref. [26]. Different from the case of changing the detection position x_t , changing the object's center position has no effect on FGD. As a result, the technique of FGD can overcome the influence of relative motion between the imaging system and the object to the imaging resolution and the object's imaging with high spatial resolution can be always reconstructed by phase-retrieval method from the FGD patterns, which provides a brand-new approach of motion deblurring and is very useful to high-precision imaging systems and imaging of moving target.

In conclusion, we have given a proposal to improve the imaging resolution of shaking object using ghost imaging technique. Both analytical and experimental results have shown that the object's shaking has no effect on the imaging resolution of FGD and the object's imaging with high spatial resolution can be always reconstructed from the FGD patterns. This technique has a great application in practice to overcome motion blur.

The work was supported by the Hi-Tech Research and Development Program of China under Grant Project No. 2011AA120101, No. 2011AA120102.

-
- [1] G. Olson, Proc. SPIE **4567**, 153 (2002).
 - [2] A. G. Lureau, Proc. SPIE **2023**, 65 (1993).
 - [3] R. C. Gonzalez and R. E. Woods, *Digital Image Processing*(2nd Edition) (Prentice Hall, 2002).
 - [4] N. Wiener, *Extrapolation, Interpolation, and Smoothing of Stationary Time Series* (MIT Press, 1964).
 - [5] R. L. Lagendijk, J. Biemond, and D. E. Bokee, IEEE Transactions on acoustics, speech, and signal processing **36**, 1874 (1988).
 - [6] K. C. Tan, H. Lim, and B. T. G. Tan. Graphical models and image processing **53**, 491 (1991).
 - [7] R. G. Lane and R. H. T. Bates, J. Opt. Soc. Am. A, **4**, 180 (1987).
 - [8] R. G. Lane, J. Opt. Soc. Am. A, **9**, 1508 (1992).
 - [9] A. Rav-Acha and S. Peleg, Pattern Recognition Letters **26**, 311 (2005).
 - [10] D. V. Strelakov, A. V. Sergienko, D. N. Klyshko, and Y. Shih, Phys. Rev. Lett. **74**, 3600 (1995).
 - [11] P. H. S. Ribeiro, S. Padua, J. C. Machado da Silva, and G. A. Barbosa, Phys. Rev. A **49**, 4176 (1994).
 - [12] R. S. Bennink, S. J. Bentley, and R. W. Boyd, Phys. Rev. Lett. **89**, 113601 (2002).
 - [13] D. Zhang, X. Chen, Y. Zhai, and L. Wu, Opt. Lett. **30**, 182354 (2005).
 - [14] A. Gatti, M. Bache, D. Magatti, E. Brambilla, F. Ferri, and L. A. Lugiato, J. Mod. Opt. **53**, 739 (2006).
 - [15] A. Gatti, E. Brambilla, M. Bache, and L. A. Lugiato, Phys. Rev. Lett. **93**, 093602 (2004).
 - [16] M. D. Angelo, and Y. H. Shih, Laser. Phys. Lett. **12**, 567 (2005).
 - [17] J. Cheng and S. Han, Phys. Rev. Lett. **92**, 093903 (2004).
 - [18] Y. Zhai, X. Chen, D. Zhang, and L. Wu, Phys. Rev. A **72**, 043805 (2005).
 - [19] J. Xiong, D. Cao, F. Huang, H. Li, X. Sun, and K. Wang, Phys. Rev. Lett. **94**, 173601 (2005).
 - [20] M. Zhang, Q. Wei, X. Shen, Y. Liu, H. Liu, J. Cheng, and S. Han, Phys. Rev. A **75**, 021803(R) (2007).
 - [21] G. Ying, Q. Wei, X. Shen, and S. Han **281**, 5130 (2008).
 - [22] H. Wang and S. Han, Europhys. Lett. **98**, 24003 (2012).
 - [23] W. Gong, P. Zhang, X. Shen, and S. Han, Appl. Phys. Lett. **95**, 071110 (2009).
 - [24] W. Gong and S. Han, arXiv:0911.4750 [Quant-ph].
 - [25] C. Zhao, W. Gong, M. Chen, E. Li, H. Wang, W. Xu, and S. Han, arXiv:1203.3835 [physics.optics].
 - [26] H. Liu, J. Cheng, and S. Han, J. Appl. Phys. **102**, 103102 (2007).